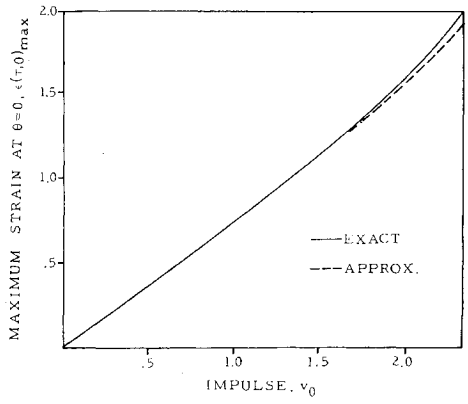

Fig. 3 Comparison of the approximate solution for the maximum strain at $\theta = 0$ with the exact solution.

The pertinent x_{i0} follow from Eqs. (10) and (13). These functions become

$$x_{i0} = (u_i/\omega_{i0}) \sin\omega_{i0}\tau \tag{14}$$

The x_{i1} differential equations are determined from Eqs. (6) and (10) and can be found in Sweet.[8] The ω_{ij} appearing in these equations must be chosen so as to eliminate the secular terms. As is demonstrated in Sweet, the elimination of the secular terms requires

$$\omega_{01}^2 = \tfrac{3}{2}\sum_{i=0} u_i^2/\omega_{i0}^2 \tag{15a}$$

$$\omega_{i1}^2 = \tfrac{3}{2}(1 + i^2)[(u_0^2/\omega_{00}^2) + \tfrac{2}{3}\omega_{01}^2 - \tfrac{1}{4}(u_i^2/\omega_{i0}^2)]$$
$$i = 1,2,4,6 \tag{15b}$$

$$\omega_{30}^2 = \omega_3^2 \equiv 10 \tag{15c}$$

$$\omega_{50}^2 = \omega_5^2 \equiv 26 \tag{15d}$$

The ω_{ij} can therefore be found from Eqs. (15) and the following equations:

$$\omega_i^2 = \omega_{i0}^2 + C\omega_{i1}^2; \qquad i = 0,1,2,4,6 \tag{16}$$

Equations (4, 8, 10, and 14) yield the solution for $\epsilon(\tau,\theta)$. This solution may be written as

$$\epsilon(\tau,\theta) = \sum_{i=0} \left\{ \frac{u_i}{\omega_{i0}} \sin\omega_{i0}\tau + \frac{1}{\omega_{i0}} \int_0^\tau \sin\omega_{i0}(\tau - \xi)[-\omega_{i1}^2 x_{i0} + f_i(x_{j0})]d\xi \right\} \cos i\theta \tag{17}$$

where all of the x_{k0} appearing in Eq. (17) are functions of the dummy variable ξ, the $f_i(x_{j0})$ can be found from Eqs. (6) and (10), and the ω_{ij} are given by Eqs. (15) and (16).

The impulsive response of the ring $\epsilon(\tau,\theta)$ subject to the half-cosine loading varies only with the parameter v_0. The parameter v_0, in turn, is related to the physical parameters of the ring by Eq. (12) and the normalized strain ϵ is related to the physical strain ϵ_θ by $\epsilon = 2(3b)^{1/2}\epsilon_\theta$.

The behavior of the system as a function of v_0 is presented in Figs. 1–3. The amplitude-frequency coupling typical of nonlinear systems is indicated in Fig. 1. The comparison of the approximate solution given by Eq. (17) to the finite difference solution of Eq. (3) at $\theta = 0$ appears in Figs. 2 and 3. The responses in Fig. 2 for $v_0 = 2.33$ and $v_0 = 1.0$ are plotted only up to the time when unloading occurs, since the stress-strain function of most materials changes during unloading. The maximum value of v_0 was chosen to be 2.33 because this value corresponds to a maximum hoop strain (ϵ_1) equal to $\bar{\epsilon}$. This value, of course, is the limiting value of Eq. (2). The maximum values of $\epsilon(\tau,\theta)$ at $\theta = 0$ vs v_0 are given in Fig. 3. It can be seen that the solution given by Eq. (17) agrees quite well with the exact solution for the maximum strain.

The method of solution developed in this study is not limited to a cubic stress-strain relationship, to the membrane equations, or to a half-cosine impulse. It can be extended to other stress-strain curves, to the more general bending equations, or to different initial conditions. This solution can also be combined with a linear analysis in order to analyze the behavior of a material behaving linearly during unloading. However, for most studies, the maximum strain appearing in Fig. 3 is all that is required.

References

[1] Payton, R. G., "Dynamic Membrane Stresses in a Circular Elastic Shell," *Journal of Applied Mechanics*, Vol. 83, Sept. 1961, pp. 417–420.

[2] Humphreys, J. S. and Winter, R., "Dynamic Response of a Cylinder to a Side Pressure Pulse," *AIAA Journal*, Vol. 3, No. 1, Jan. 1965, pp. 27–32.

[3] Roth, R. S. and Klosner, J. M., "Nonlinear Response of Cylindrical Shells Subjected to Dynamic Axial Loads," *AIAA Journal*, Vol. 2, No. 10, Oct. 1964, pp. 1788–1794.

[4] Dowell, E. H., "On the Nonlinear Flexural Vibrations of Rings," *AIAA Journal*, Vol. 5, No. 8, Aug. 1967, pp. 1508–1509.

[5] Perrone, N., "Impulsively Loaded Strain Hardened Rate-Sensitive Rings and Tubes," *International Journal of Solids and Structures*, Vol. 6, No. 8, Aug. 1970, pp. 1119–1132.

[6] Cunningham, W. J., *Introduction to Nonlinear Analysis*, McGraw-Hill, New York, 1958, pp. 129–130.

[7] Tsien, H. S., "The Poincaré-Lighthill-Kuo Method," *Advances in Applied Mechanics*, Vol. IV, 1956, p. 281.

[8] Sweet, J., "Dynamic Response of a Work Hardening Ring," SCL-DC-70-61, May 1970, Sandia Laboratories, Livermore, Calif.

Correlation of Inviscid Air Nonequilibrium Shock Layer Properties

CLARENCE J. HARRIS*

General Electric Company, Valley Forge, Pa.

Entropy Correlation-Analog

WITHIN an appropriate flight regime, an entropy correlation and a nozzle-shock layer analog may be combined to predict the frozen nonequilibrium properties in the inviscid inner shock layer stream tube for slender, slightly blunted, conical bodies. Early analytical work on flow expansions

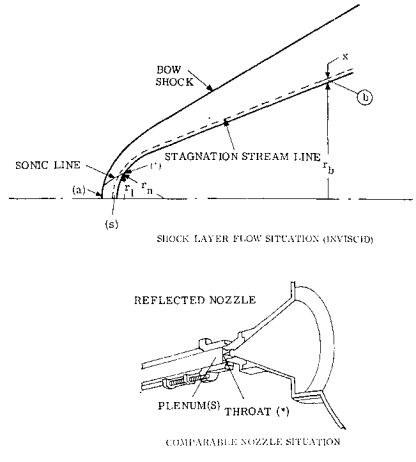

Fig. 1 Nozzle flow—shock layer analog.

Presented as Paper 70-866 at the AIAA 5th Thermophysics Conference, Los Angeles, Calif., June 29–July 1, 1970; submitted July 29, 1970; revision received November 10, 1970.

* Staff Scientist, Environmental Sciences Laboratory, RESD.

and nonequilibrium effects[1,2] showed that the nonequilibrium chemical composition in an expanding nozzle airflow could be readily correlated as a function of plenum or reservoir entropy. Harris et al.,[3,4] also showed that a similar "entropy correlation" was valid for specifying the nonequilibrium electron concentration values in an expanding air flow. Both Harney[5] and Ring and Johnson[6] have made extensions to the entropy correlation concept offered in Refs. 1 and 2. This simplified entropy correlation for handling energetic nozzle air flows has had direct application in understanding and defining hypersonic and hypervelocity test facilities performance.[7-9]

The nozzle nonequilibrium entropy correlation approach can also be adapted to the case of hypersonic shock layer flow around a blunt, slender axisymmetric body. An analog between nozzle flow and shock layer flow can be established by considering the flow situations in Fig. 1. The center body is a cone with a spherical nose. Thus, the stream tube crossing the bow shock wave at (a) is eventually stagnated at (s), and then expands to sonic velocity at (*) and becomes supersonic downstream of this point. Therefore, region (s) in the shock layer flow is analogous to the plenum region in the nozzle flow situation (see Fig. 1a), and (*) in the shock layer situation is analogous to the throat in the nozzle flow case (see Fig. 1b). Further, the supersonic expansion of the center body stream tube downstream of the sonic point is analogous to the supersonic expansion in the nozzle case. The present analysis is applicable to the center body stream tube and regions such as (s), (*), and later on (b) in the shock layer flow. It is necessary to require that the reacting stagnated air in region (s) be in equilibrium and that it undergo an equilibrium expansion to the sonic point (*).[2,7] The center body station at which the flow will depart from equilibrium and "freeze" in its nonequilibrium chemical composition may be determined on the basis of the center body bluntness ratio (B) or the equivalent annular stream tube area ratio $[A_{(b)}/A_{(*)}]$. The interdependence of these two may be approximated[4] as follows:

$$A_{(b)}/A_{(*)} \sim (x + 2r_n/B)/(x + 1.3r_n) \quad (1)$$

where

$$B = r_n/r_b \quad (2)$$

Let

$$\xi = x/r_n = f(M_\infty,h) \quad (3)$$

M_∞ being flight Mach number and h being flight altitude, then

$$A_{(b)}/A_{(*)} \sim (\xi + 2/B)/(\xi + 1.3) \quad (4)$$

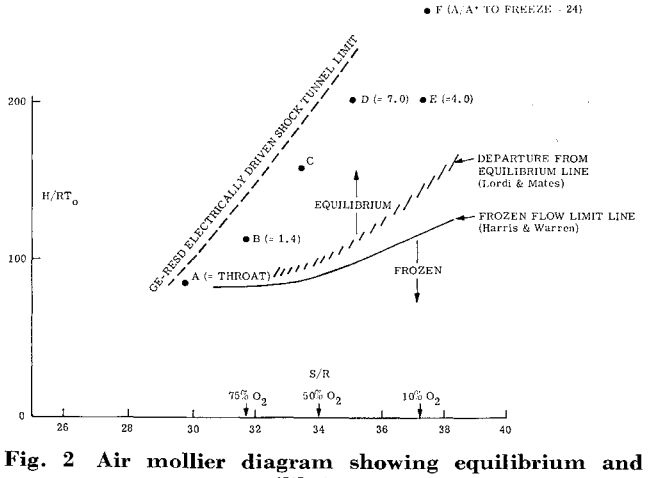

Fig. 2 Air mollier diagram showing equilibrium and nonequilibrium regime.

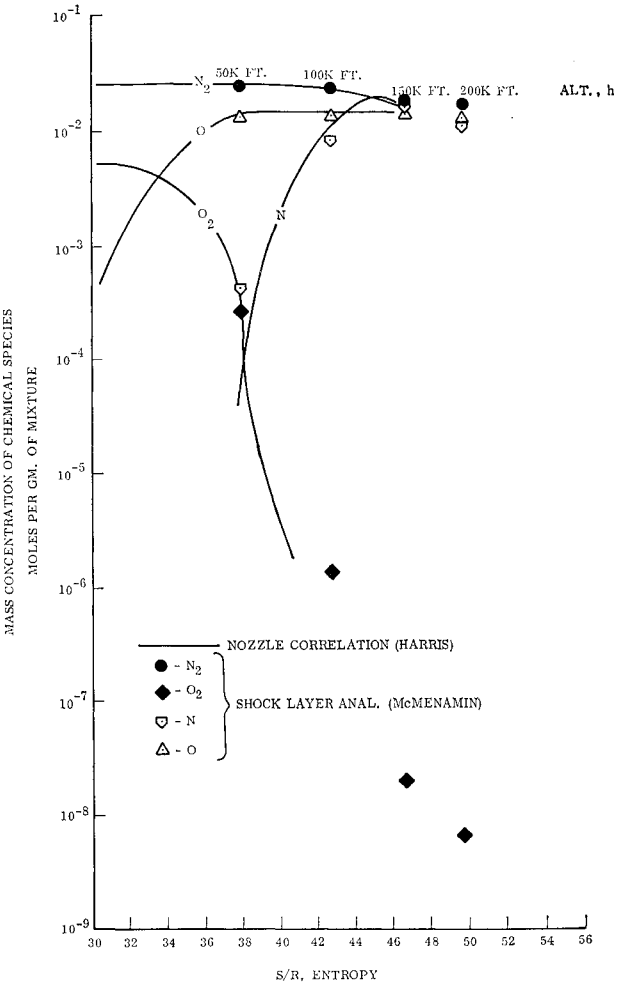

Fig. 3 Comparison of nonequilibrium shock layer chemical composition to nonequilibrium nozzle correlation.

for $\xi \ll 1$ and $B < 1$,

$$A_{(b)}/A_{(*)} \sim 2/1.3B \quad (5)$$

Application to Flight

Having the entropy correlation and the nozzle-shock layer analog, one then determines the stagnation enthalpy and entropy values at (s) for the flight conditions under consideration. If this flight point falls above the departure from equilibrium boundary on the Air Mollier Diagram (Fig. 2), then the equivalent area ratio or bluntness ratio (B) at which freezing will occur may be determined by the required isentropic equilibrium expansion to the "Frozen Flow Limit Line." Once this center body station (or area ratio) is defined, the chemical composition and electron concentration in the center body stream tube at points downstream of this station should be able to be defined based on the stagnation point entropy value.

Inviscid, nonequilibrium sphere-cone body shock layer calculations[10] were compared to the earlier nozzle results.[1] The center body configuration selected was one which had a cone angle of <10° and slight cone bluntness. Inviscid flowfield results were chosen for four flight conditions. The flowfield calculations were available for three normals along the center body surface for each of these flight conditions; the most downstream of these normals is at a body station yielding an equivalent area ratio value of approximately 50, thus well into the frozen nonequilibrium flow regime on the body. Figure 3 shows the numerically calculated shock layer chemical composition for the center body stream tube (sym-

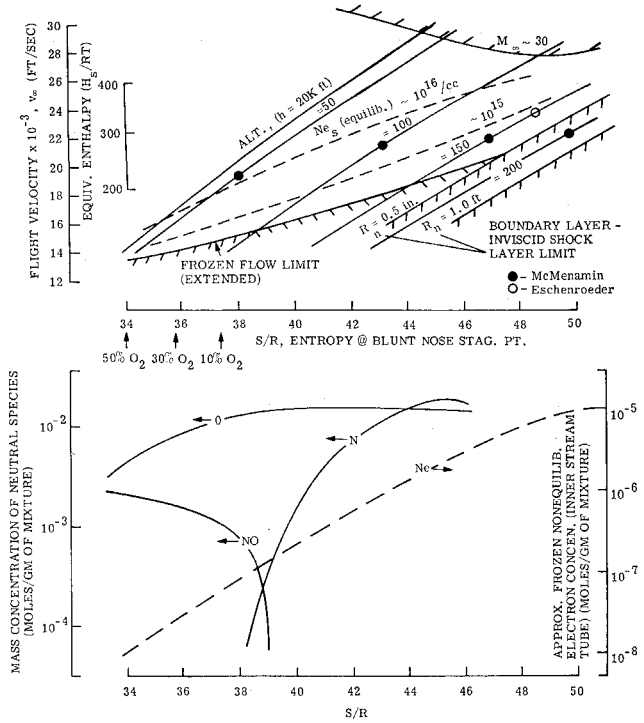

Fig. 4 Correlation and prediction of shock layer properties as a function of flight conditions.

bols) at this body station for the four flight conditions as compared to the composition based on the nozzle entropy correlation (solid lines).[1,2] The species considered are O_2, N_2, O and N. With the exception of the order of magnitude disagreement between the calculated value of N and the value for N predicted by the correlation at the 50-k ft condition, the overall agreement is quite good, and the correlation appears to predict the chemical properties in the frozen nonequilibrium portion of the inviscid center body stream tube quite well.

Figure 4 presents the entropy correlation of shock layer flow properties as a function of vehicle flight conditions. Flight velocity (v_∞) and center body stream tube stagnation point enthalpy (H_s/RT_0) are presented vs entropy (S/R). Lines of constant flight altitude (h) and stagnation point electron density [$Ne_{s(\text{equilib.})}$] are also included. The four flight conditions that were used are shown (filled circles) as well as the flight point from Ref. 11 (open circle).[4] The altitude boundaries for achieving a viscous boundary-layer inviscid shock layer flow are presented for both a 0.5 in. and 1.0-ft nose radius center body. The other limit line is the frozen line.[2,4,7] Presented below the flight condition plot in Fig. 4 is a replot of the entropy correlation of neutral species and electron concentration. One need only to use the top half of Fig. 4 to determine the stagnation point entropy value at any given point on a flight trajectory (v_∞ and h). Then, by projecting straight down along this entropy value to the curves below, an estimate of the electron concentration is obtained as well as fairly accurate quantitative values of the neutral chemical species concentration. Thus, for example, a vehicle at 100-k ft altitude and flying at 25,000 fps is predicted to have a downstream center body stream tube electron density value of 3×10^{-6} (mol/g mix.) and the neutral chemical species composition specified at the entropy (S/R) value of 46. The stagnation point equilibrium electron density value will be 10^{16} electrons/cm^3.

The applicability of this shock layer prediction technique is as shown in Fig. 4. Therefore, the prediction technique is generally applicable from h = 200-k ft for v_∞ between 22 to 33-k fps to h = 50-k for v_∞ between 12-k fps to 30-k fps.

References

[1] Harris, C. J., "Comment on Nonequilibrium Effects on High-Enthalpy Expansion of Air," *AIAA Journal*, Vol. 4, No. 6, June 1966, pp. 1148–1149.

[2] Harris, C. J. and Warren, W. R., "Correlation of Nonequilibrium Chemical Properties of Expanding Air Flows," R64SD92, Dec. 1964, General Electric Co., Valley Forge, Pa.

[3] Harris, C. J., Marston, C., and Warren, W. R., "MHD Generator and Accelerator Experiments in Seeded and Unseeded Air Flows," R66SD50, Sept. 1966, General Electric Co., Valley Forge, Pa.

[4] Harris, C. J., "Correlation of Inviscid Air Nonequilibrium Shock Layer Properties," R68SD333, Dec. 1968, General Electric Co., Valley Forge, Pa.

[5] Harney, D. J., "Similarity of Nonequilibrium Expansions in Hypersonic Nozzles," FDM-TM-67-1, May 1967, Wright-Patterson Air Force Base, Ohio.

[6] Ring, L. E. and Johnson, P. W., "Correlation and Prediction of Air Nonequilibrium in Nozzles," AIAA Paper 68-378, San Francisco, Calif., 1968.

[7] Marston, C. H. and Warren, W. R., "Study of a Continuous Discharge Driver/Non-Reflected/Free Piston Shock Tunnel," *AIAA Journal*, Vol. 7, No. 5, May 1969, pp. 964–967.

[8] Warren, W. R. and Harris, C. J., "A Critique of High-Performance Shock Tube Driving Techniques," TR-0066 (5240-10)-6, Sept. 1969, Aerospace Corp., El Segundo, Calif.

[9] Leonard, R. L. and Rose, P. H., "Feasibility of a High Performance Aerodynamic Impulse Facility," *AIAA Journal*, Vol. 6, No. 3, March 1968, pp. 448–457.

[10] McMenamin, D. and O'Brien, M., "The Finite Difference Solution of Multicomponent Nonequilibrium Steady Influscid Stream Tube Flows Using a Novel Stepping Technique," 67SD-241, April 1967, General Electric Co., Valley Forge, Pa.

[11] Eschenroeder, A. Q., "Ionization Nonequilibrium in Expanding Flows," *ARS Journal*, Vol. 31, No. 2, Feb. 1961, pp. 196–203.

Amplification by Wave Distortion in Unstable Combustors

M. F. Heidmann*

NASA Lewis Research Center, Cleveland, Ohio

Nomenclature

C_1	=	proportionality constant
c	=	speed of sound
D	=	drop diameter
n	=	harmonic order
P'	=	pressure perturbation
p_1,p_2	=	harmonic coefficients for P'
Re	=	Reynolds number of drop
$\Re$	=	response (burning rate perturbation in-phase with pressure oscillation) described by Eq. (5)
t	=	time
U	=	magnitude of relative drop velocity vector
u_l	=	axial velocity of drop
u_z,u_θ,u_r	=	gas velocity in axial, tangential and radial directions
W,W'	=	normalized drop burning rate (actual and perturbation)
w,w_0	=	drop burning rate (actual and initial value)
γ	=	ratio of specific heats
$\rho,\bar{\rho},\rho'$	=	gas density (actual, mean value and perturbation)
φ_2	=	phase relation between first and second harmonic components
φ_u	=	phase relation between pressure and acoustic particle velocity
μ	=	gas viscosity

Received September 2, 1970; revision received October 15, 1970.

* Aerospace Scientist. Member AIAA.